Causal relationships between frequency bands of extracellular signals in visual cortex revealed by an information theoretic analysis. Online resource 1

M Besserve*, B. Schölkopf, N. K. Logothetis and S. Panzeri

Simulation study

Henon maps

Following (Quiroga et al, 2000), we tested whether NTE was dependent on the respective complexity of two interacting systems. We simulated a system of coupled Henon maps following the equations

$$\begin{cases} x(t+1) = & 1.4 - x(t)^2 + .3\ u(t) \\ u(t+1) = & x(t) \end{cases}$$

$$\begin{cases} y(t+1) = & 1.4 - (Cx(t) + (1-C)y(t))y(t) + B\ v(t) \\ v(t+1) = & y(t) \end{cases}$$

The strength of the unidirectional coupling from X to Y is given by the parameter C. Similar to Quiroga and colleagues (Quiroga et al, 2000), we computed NTE for identical (B=.3) and non-identical (B=.1) subsystems. According to the authors, this enables to see the influence of the complexity of the subsystems on the measure. Results are summarized on Supplementary Fig 1. Panel a shows that for two identical systems, the coupling direction can be retrieved from NTE values: NTE is large in the good direction and almost vanishes in the wrong direction. We observe that in the case of strong coupling, NTE values in the wrong direction slightly increases, suggesting that strong coupling tends to reduce asymmetry of the measure. On Supplementary Fig 1. Panel b, we also observe that directionality of the coupling is easily found, whereas the overall value of NTE is largely increasing compared to the symmetric case. This shows that finding the direction of causation with our approach is not sensitive to the difference in complexity of the two systems.

Finally, we observe in all cases, that NTE is decreasing for large time delay parameters until it vanishes. The inequality between NTE values in both directions is preserved for a wide range of delay parameter, showing it is not very sensitive to the choice of this hyper-parameter.

Two frequencies, linear system

We investigated the behavior of causality measures for signals in a narrow frequency band. We simulated the following linear system composed of two coupled auto-regressive processes, generated by linear filtering (Auto-regressive Moving Average) of two white noise signals:

$$X(t) = 2r\cos(2\pi f_x/F_e)X(t-1) - r^2X(t-2) + \varepsilon(t-1) - \varepsilon(t-2) \qquad (1)$$

$$Y(t) = 2r\cos(2\pi f_y/F_e)Y(t-1) - r^2Y(t-2) + \nu(t-1) - \nu(t-2) + .\mathbf{01X(t-1)} \qquad (2)$$

$F_e = 1000$Hz is the sampling frequency, ε and ν are Gaussian white noises of variance 1. The spectrum of X (respectively Y) is centered around the frequency f_x (resp f_y). The constant r=.9 controls the selectivity of the bandpass filter. According to the coupling term in bold, there is a causal influence from X to Y. We computed NTE on these simulated signals in both directions ($X \to Y$ and $Y \to X$) for two possible center frequencies of each signal (50Hz and 80Hz) corresponding to empirical centered frequencies for low and high gamma activity. The results are reported on Supplementary Fig. 2(a). We observe that for small time delays, NTE in the direction $Y \to X$ does not vanish when conditioning on one time delay, but is lower than the NTE value in the opposite direction. In the good direction $X \to Y$, we observe oscillations in the NTE pattern as a function

*Max Planck Institute for Biological Cybernetics, Tuebingen, Germany. michel.besserve@tuebingen.mpg.de

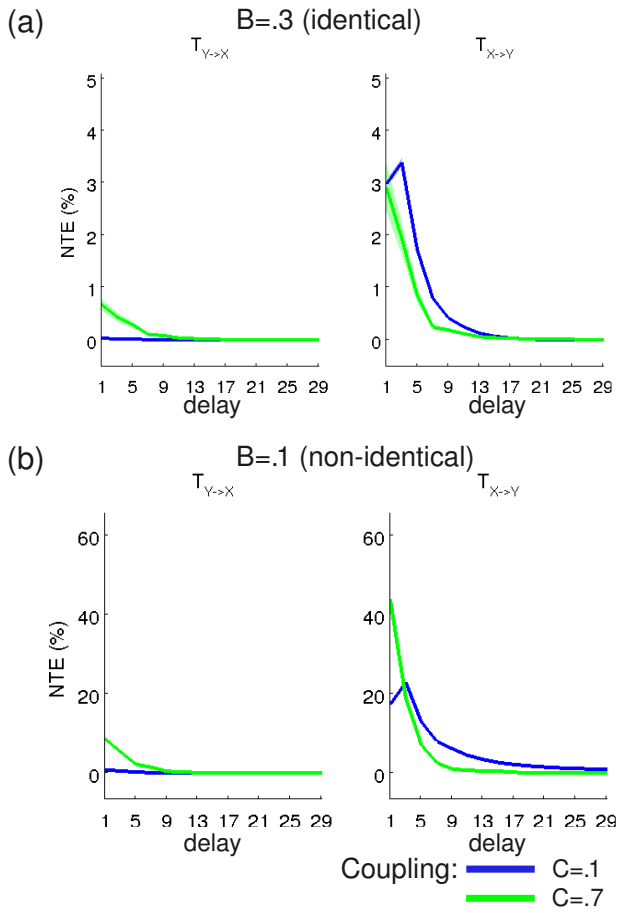

Supplementary Fig. 1: **NTE values for coupled Henon maps** for weak (C=.1) and strong (C=.7) coupling, as a function of the time delay parameter. Areas around the curves indicate standard deviation across simulation trials. (**a**) case of two identical systems (B=.3). (**b**) case of non-identical systems (B=.1)

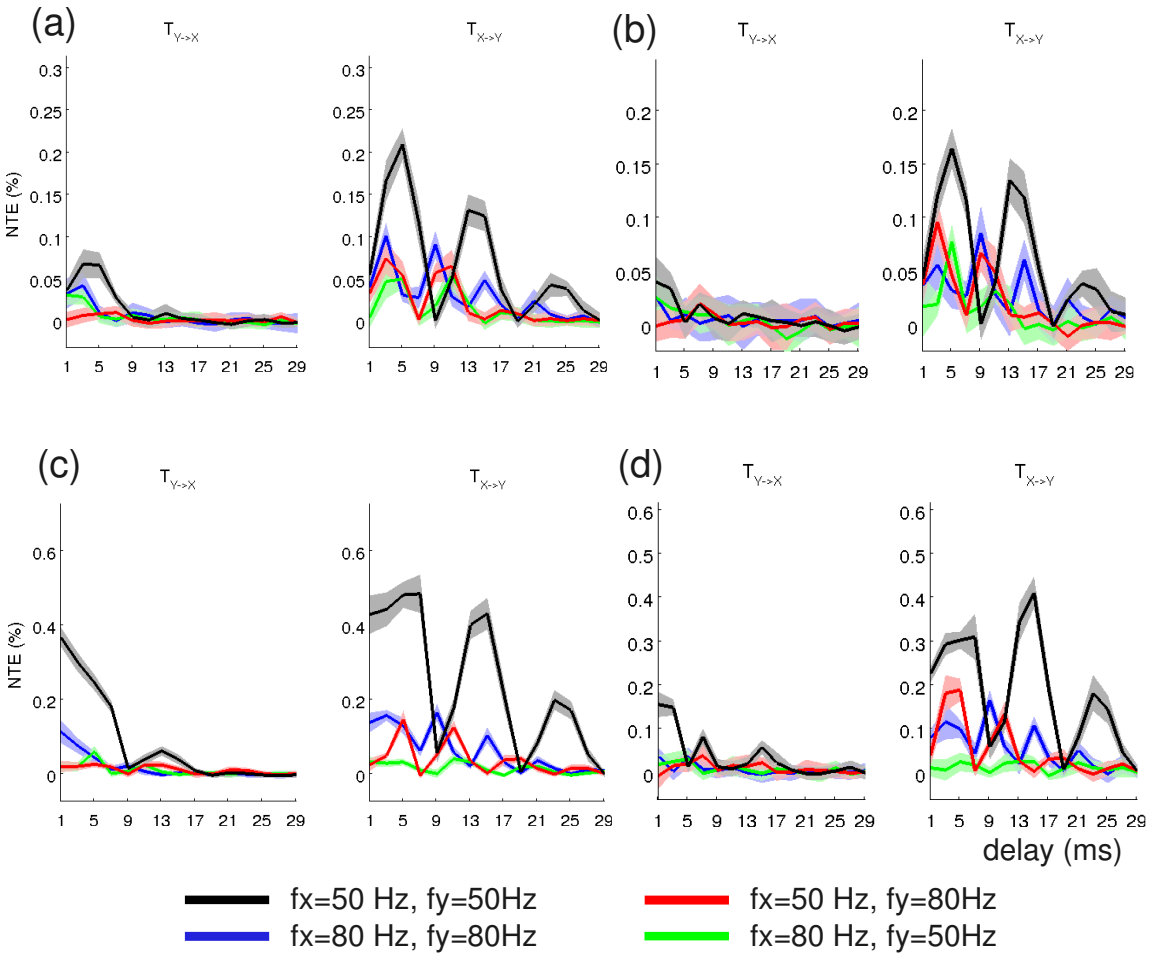

Supplementary Fig. 2: **NTE values for a linear system of coupled oscillators** X and Y of frequency f_x and f_y respectively. Results for causality in both directions ($X \to Y$ and $Y \to X$) are plotted as a function of the time delay in different cases. Areas around the curves indicate standard deviation across simulation trials. (**a**) NTE values computed on unfiltered signals by conditioning on one time delay. (**b**) NTE values computed on unfiltered signals by conditioning on two time delays (τ and 2τ). (**c**) NTE values computed on band-pass filtered signals by conditioning on one time delay. (**d**) NTE values computed on band-pass filtered signals by conditioning on two time delays.

of the delay. We tested whether the positive NTE in the wrong direction was a consequence of insufficient conditioning on past values. When conditioning on two time delays (Supplementary Fig. 2(b), NTE in the wrong direction is reduced, at the expense of an increase in the variance of the estimator. Still we observe fluctuations in NTE values in the good direction. When interacting oscillations have the same center frequency, the period of these fluctuations is half the period of the oscillations. When the oscillations have a different frequency, no simple relationship between fluctuations and the original period of the oscillations can be observed.

We further tested the effect of filtering these signals in narrow bands, as can be done in practice to isolate activities in different frequency bands. As shown in Supplementary Fig. 2(c) and (d), for interactions within the same frequency band, this has for consequence to increase NTE in both directions. We still observe that the NTE value in the good direction remains larger. For interactions between different frequency bands in the good direction $X \to Y$, NTE from 50 to 80Hz tends to increase after filtering, but NTE from 80 to 50Hz tends to slightly decrease. The consequence is that NTE is still higher in the good direction when information transfer goes from 50 to 80Hz, but NTE has equivalent value in both directions when information transfer goes from 80 to 50Hz. According to this simulation study, NTE of filtered signals could be biased toward the direction from low frequencies to higher frequencies. To gain in generality, this point requires to be further investigated. In particular non-linear models of cross-frequency interactions should be studied with the same approach, but to our knowledge, such models are lacking in the literature (at least for discrete-time systems).

Linking TE with phase synchronization

We computed n:m phase synchronization to compare this measure to Transfer entropy. Since phase synchronization is restricted to the analysis of narrow band signals (Chavez et al, 2006), we restricted this analysis to low gamma and high gamma band signals (at high resolution). Phase synchronization was computed by extracting the phase of each signal by Hilbert transform and then by computing the phase locking value (PLV) (Lachaux et al, 1999; Schack et al, 2005):

$$PLV(1,2) = |1/K \sum_{k=1}^{K} \exp(\mathbf{i}(n\varphi_1(k) - m\varphi_2(k)|$$

The integers n and m where chosen as a function of the center frequency of the respective signals. For equal frequencies, n=m=1. For different frequencies, the ratio n/m corresponds to the ratio of center frequencies. So if the first signal is low gamma (50Hz) and the second high gamma (80Hz), we choose n=8 and m=5. Conversely, if the first signal is high gamma (80Hz) and the second low gamma (50Hz), we choose n=5 and m=8. We then compared the phase locking value with its corresponding transfer entropy value. We thus computed the Spearman's rank correlation coefficient between PLV and NTE values computed from the low and high gamma band signals. The results are plotted on Supplementary Fig 3. Panel a shows, that PLV correlates with NTE measured on raw gamma oscillations for some sessions when the interactions are within the same frequency band, especially in the low gamma band. For cross-frequency interactions, no clear correlation in found. When NTE is measured directly on the phase of gamma oscillations, Supplementary Fig 3 Panel b, shows that the previously observed correlations for interactions in the same band are more pronounced. Panel c shows that for some sessions (d04nm1), the relationship between phase synchrony and phase Transfer Entropy is almost deterministic.

The above results show that, on this data set, phase synchrony values and Transfer Entropy values covariate when interactions are measured in the same narrow band. The effect is more pronounced when TE is computed on the phase of the signals since interfering effects of the changes in signal amplitude are removed. Nevertheless, we want to emphasize that it is not because these two measures covary that they are identical. One trivial illustration of their difference is the case of two identical oscillatory signals: whereas phase synchrony analysis will conclude that the two systems are highly synchronized, Transfer entropy will just vanish because the two signals carry exactly the same information. Moreover, whereas phase synchrony analysis is restricted to periodic phenomena or narrow band signals, Transfer Entropy can be applied in more general cases. Finally, in our case, TE values for cross-frequency interactions can not be explained by n:m phase synchronization measures.

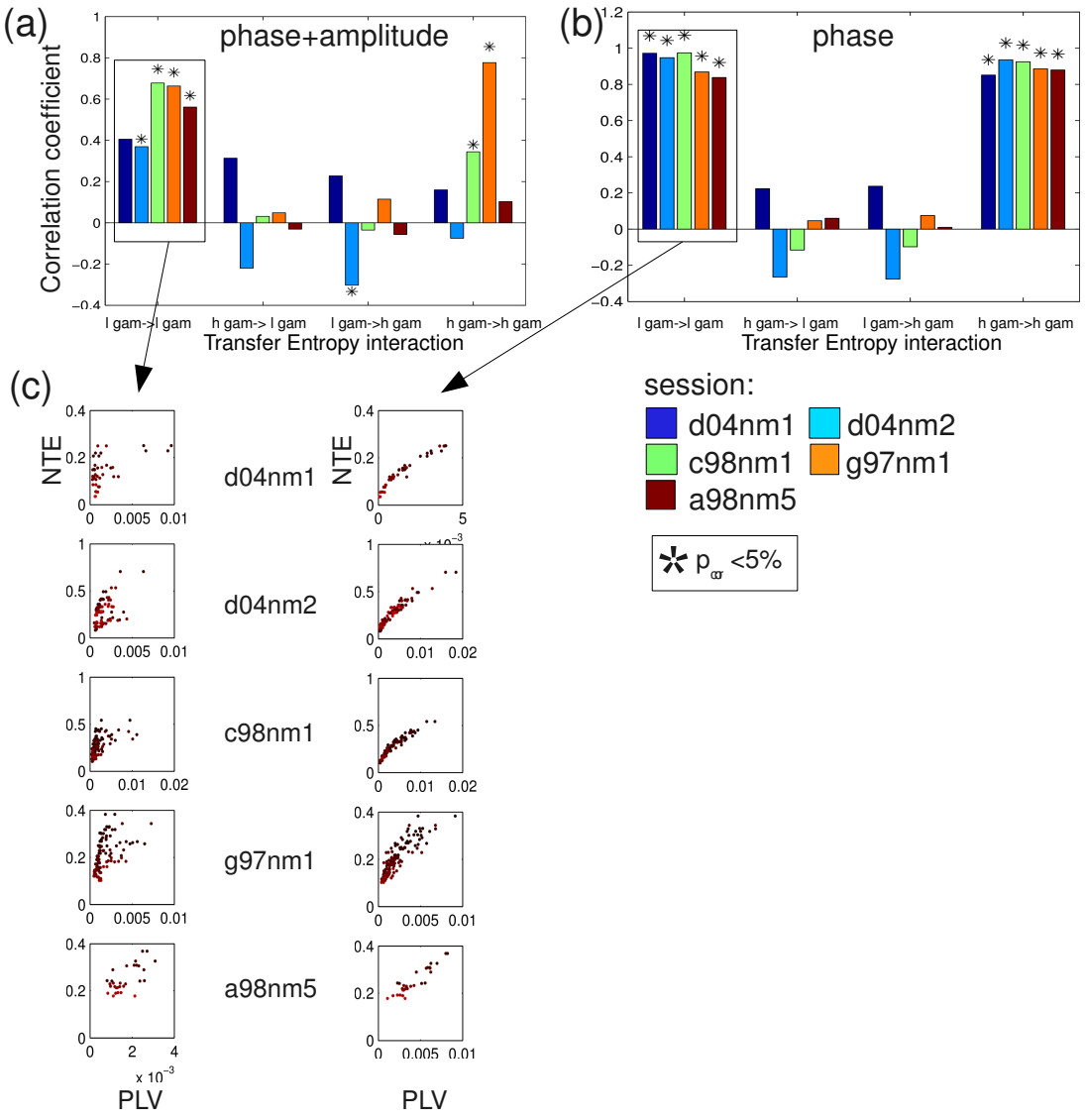

Supplementary Fig. 3: **Correlation between NTE values and PLV values** for distant interactions within the low and high gamma bands. (**a**) Spearman correlation coefficient between PLV and NTE across all couples of recording sites, results are given for all sessions and directions of causality. NTE is computed from the raw gamma oscillations (thus including phase and amplitude information). (**b**) Same as (a) but NTE is computed from the phase of gamma oscillations. (**c**) Scatter plot of NTE and PLV values (across all couples of recording sites) for interactions within the low gamma band related to correlation coefficients in the previous panels. The color of points indicates the distance between the recording sites (black: 6mm, red:1mm).

Supplemental result: Bootstraped NTE statistics at low temporal resolution

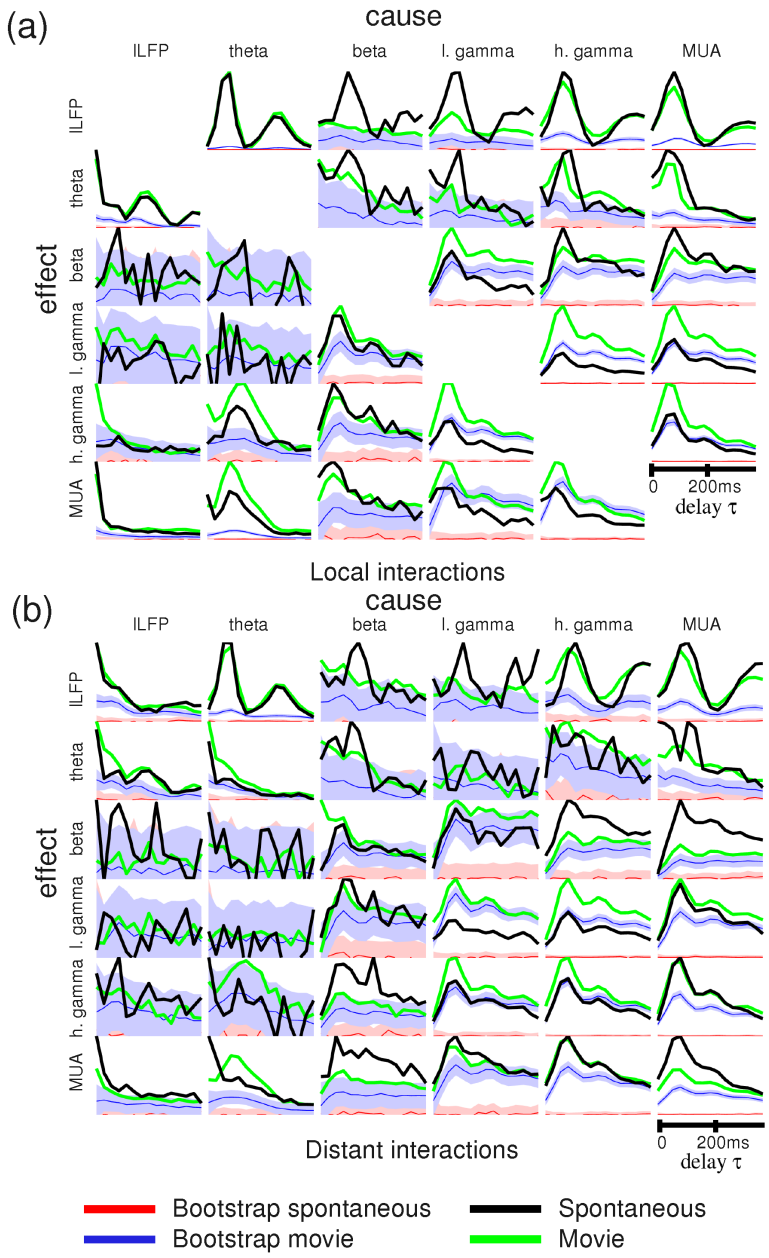

Supplementary Fig. 4: **Bootstraped NTE statistics** for causal interactions between frequency bands at low temporal resolution (low pass filtered to $F = 8Hz$, cf. Table 1), as a function of the delay parameter (τ). Average value of $NTE^{cor}_{\text{cause}\to\text{effect}}$ across the whole dataset (all monkeys, all movies and all recording sites) is plotted as a function of the delay τ for two conditions: movie stimulation (green curve) and spontaneous activity (black curve). Blue and red curves indicate the corresponding average of bootstrap estimates for the same subset of electrodes. The shaded area indicates the average standard deviation of the statistics around the mean. (**a**) **Local interactions**, the average is taken between all NTE values of signal from the same electrode. (**b**) **Distant interactions**, the average is taken between all NTE values of signals originating from any two different electrodes.

Supplemental result: Causal interactions between frequency bands at low and middle temporal resolution

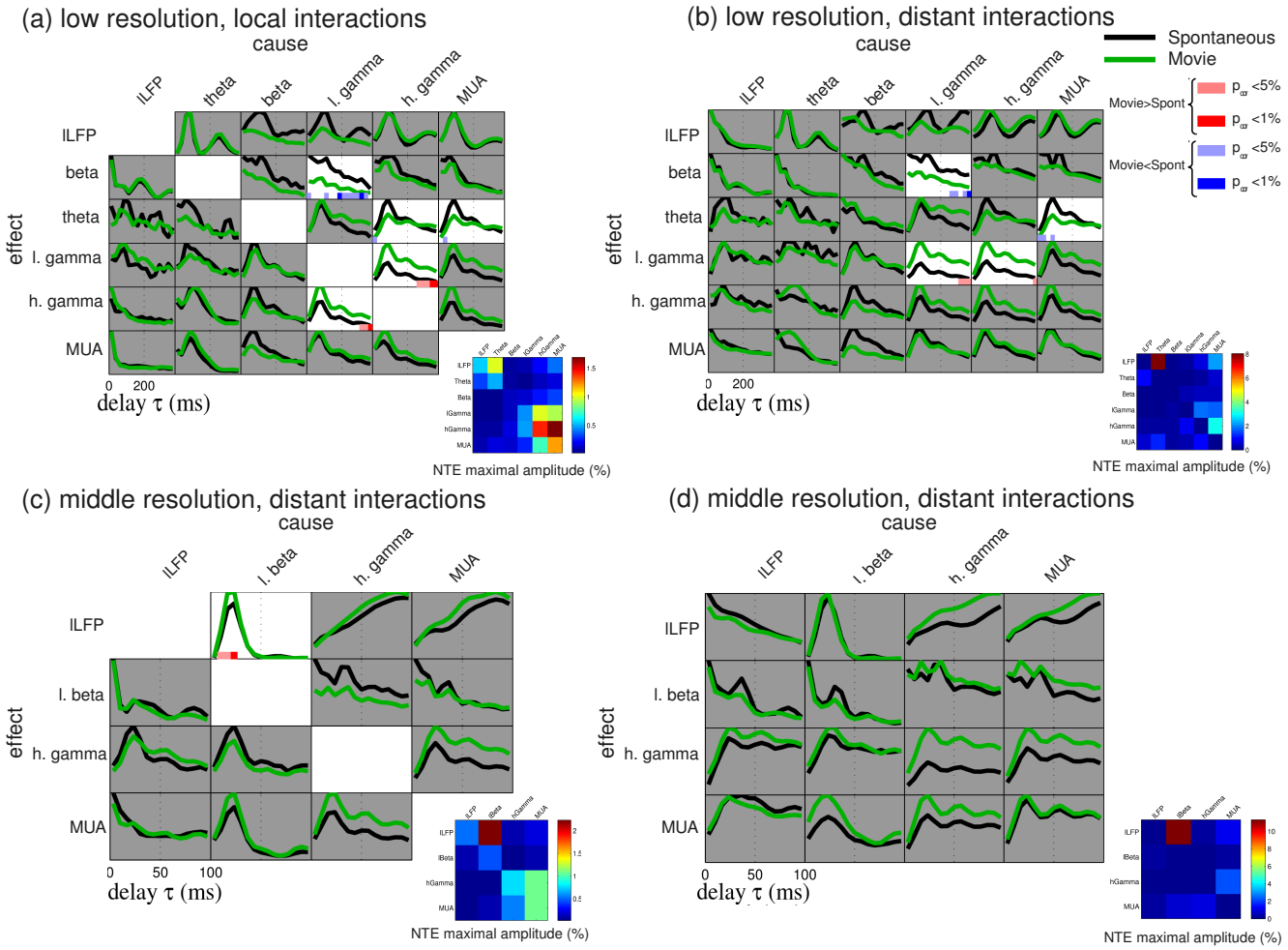

Supplementary Fig. 5: **Causal interactions between frequency bands at low and middle temporal resolution** (low pass filtered to 8Hz and 30Hz respectively, cf. Table 1), as a function of the delay parameter (τ). Average value of $NTE^{cor}_{cause \to effect}$ across all monkeys and recording sites is plotted as a function of the delay τ for two conditions: movie stimulation (green curve) and spontaneous activity (black curve). Red and blue horizontal lines indicate the delays for which the difference between conditions is significant. Columns in each table correspond to the cause frequency and rows to the effect frequency. For each panel, the colored grid on the bottom right hand side indicates the maximal NTE value of the considered pair of frequencies over the entire τ range shown in the corresponding left-hand side plots. Gray background indicates no significant effect for all delays. (**a**) average NTE for **local interactions** (in the same electrode) at low temporal resolution. (**b**) average NTE for **distant interactions** between different recording sites at low temporal resolution. (**c**) average NTE for **local interactions** (in the same electrode) at middle temporal resolution. (**d**) average NTE for **distant interactions** between different recording sites at middle temporal resolution.

Supplemental result: Robustness of NTE changes at high temporal resolution

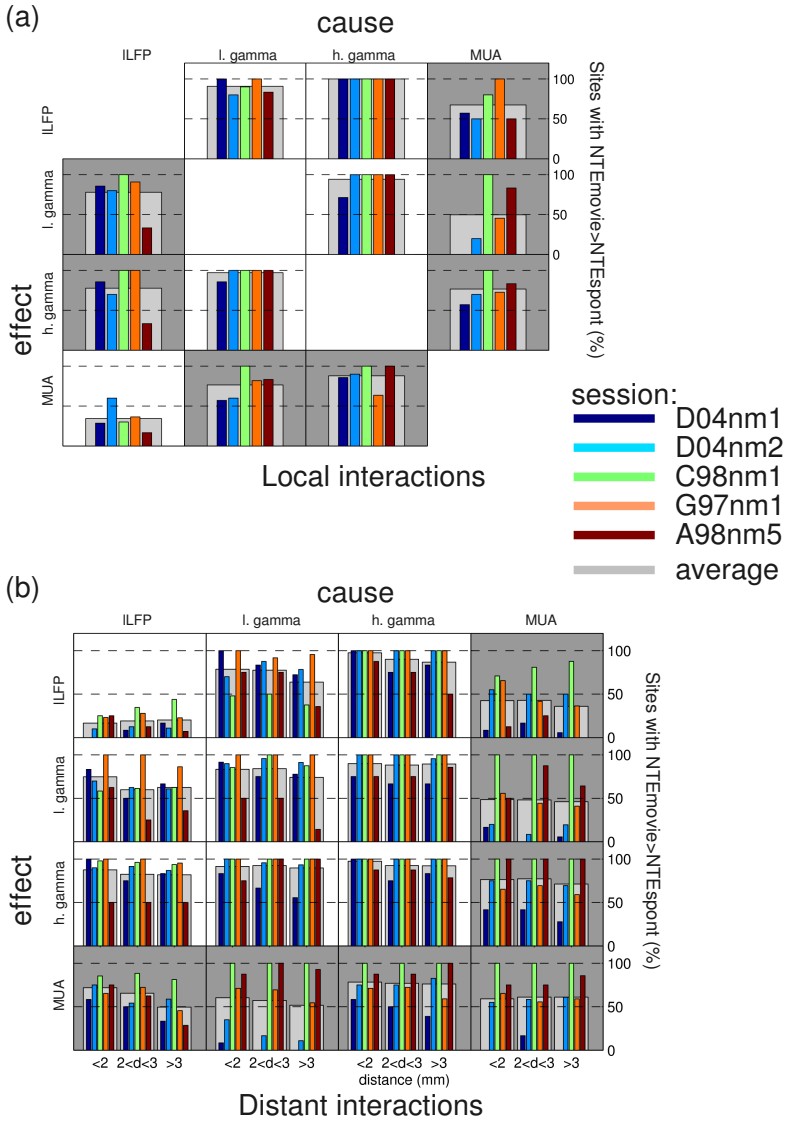

Supplementary Fig. 6: **Robustness of NTE changes at high temporal resolution** estimated by the proportion of recording sites with increasing average NTE during movie stimulation (compared to spontaneous activity). Shaded plots indicate couples of frequencies with no significant effect of the stimulus. Colored bars indicate the proportion for each recording session and the average across all sessions is plotted in gray. (**a**) causality within the same recording site. (**b**) causality between different electrodes. For (b), the percentage is plotted as a function of the distance between sites: low distance ($\leq 2mm$), intermediate ($2 < dist \leq 3mm$) and large ($> 3mm$).

Supplemental result: Robustness of NTE changes at low temporal resolution

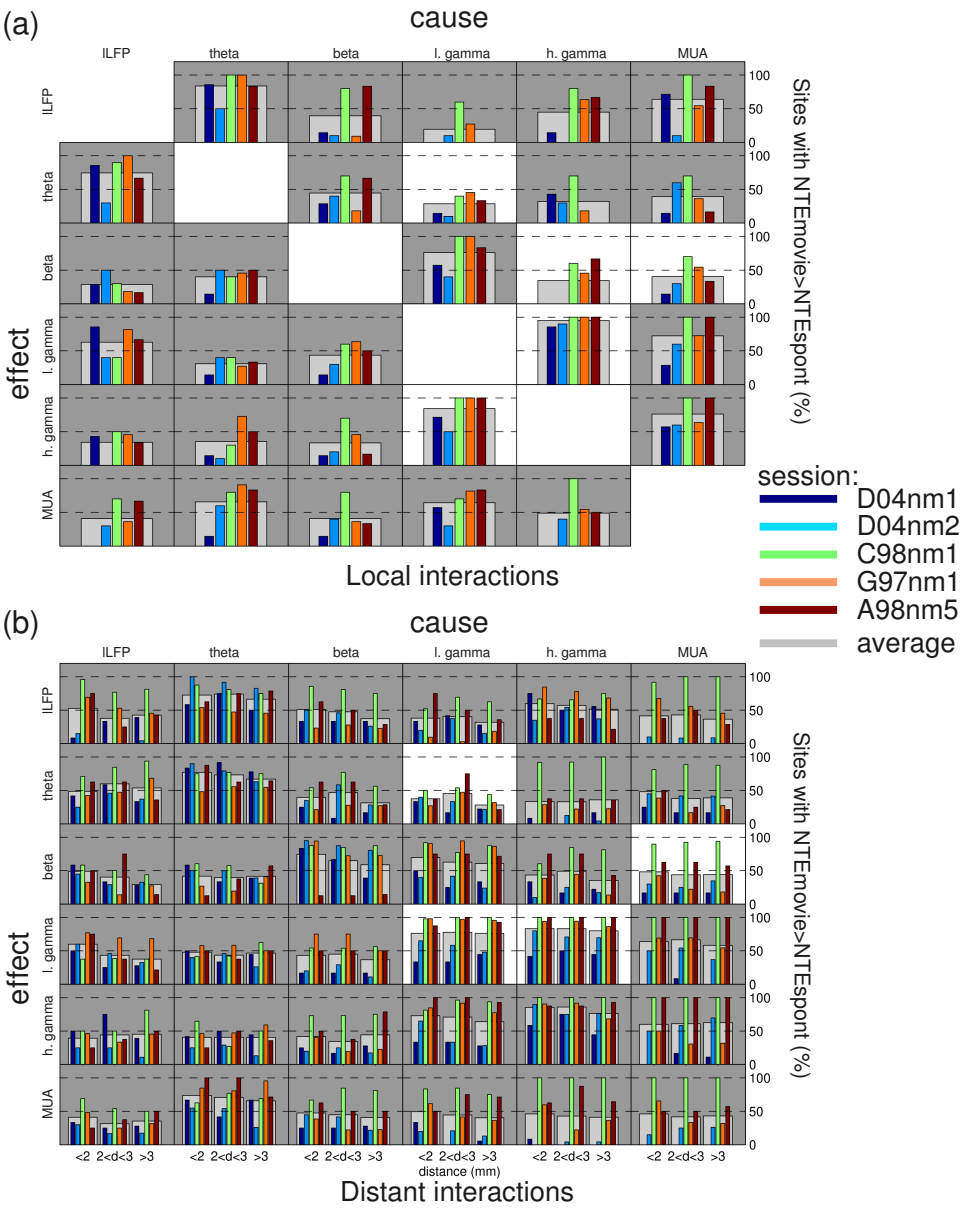

Supplementary Fig. 7: **Robustness of NTE changes at low temporal resolution** estimated by the proportion of recording sites with increasing average NTE during movie stimulation (compared to spontaneous activity). The results are shown for couples of frequencies with significant effect of the stimulus. Colored bars indicate the proportion for each recording session and the average across all sessions is plotted in grey. (**a**) causality within the same recording site. (**b**) causality between different electrodes. For panel b, the percentage is plotted as a function of the distance between sites: low distance ($\leq 2mm$), intermediate ($2 < dist \leq 3mm$) and large ($> 3mm$).

Supplemental result: Power spectral density of analyzed signals

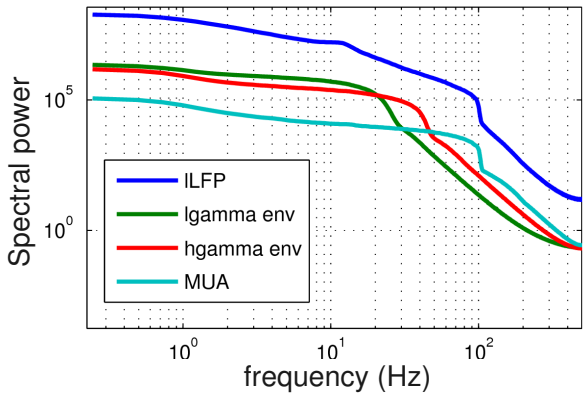

Supplementary Fig. 8: Power spectrum of signal in various frequency bands averaged across electrodes and experiments for one session (A98nm5). Estimation is made with a Welch Periodogram

Supplemental result: Joint distribution distance/NTE

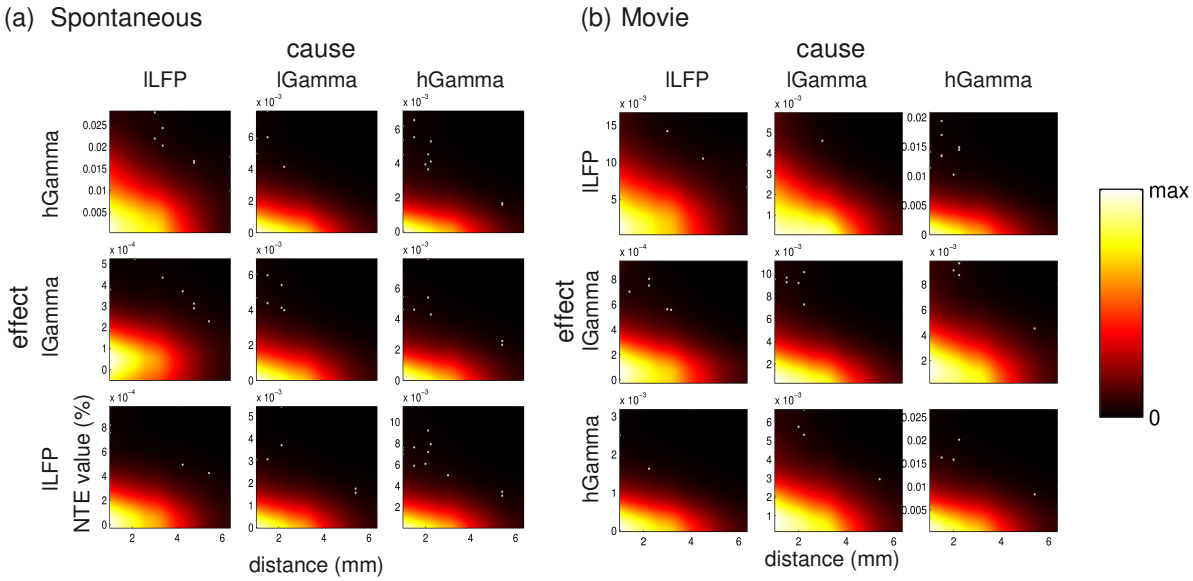

Supplementary Fig. 9: Smoothed histogram of the joint distribution (distance, NTE value) for several couples of frequency bands in spontaneous activity (a) and movie stimulation (b). White points indicate outliers that in areas where the smoothed density is less than 5% of the maximal density.

References

Chavez M, Besserve M, Adam C, Martinerie J (2006) Towards a proper estimation of phase synchronization from time series. J Neurosci Methods 154:149–160

Lachaux J, Rodriguez E, Martinerie J, Varela F (1999) Measuring phase synchrony in brain signals. Hum Brain Mapp 8:194–208

Quiroga RQ, Arnhold J, Grassberger P (2000) Learning driver-response relationships from synchronization patterns. Phys Rev E 61:5142–5148

Schack B, Klimesch W, Sauseng P (2005) Phase synchronization between theta and upper alpha oscillations in a working memory task. Int J Psychophysiol 57:105 – 114